Available online at www.sciencedirect.com

ScienceDirect

Solar Energy 126 (2016) 137–145

SOLAR ENERGY

www.elsevier.com/locate/solener

On-line fault detection algorithm of a photovoltaic system using wavelet transform

il-Song Kim *

Department of Electrical Engineering, Korea National University of Transportation, Republic of Korea

Received 20 October 2015; received in revised form 4 December 2015; accepted 6 January 2016
Available online 16 January 2016

Communicated by: Associate Editor Mario Medina

Abstract

The fault detection algorithm of a grid-connected photovoltaic system using wavelet transform is suggested in this paper. When the faults occur in the power conditioning system, the impact on the grid system is very risky. Therefore, it is necessary to detect faults in a short time period. When using the conventional detection method, extra hardware and sensors are required to detect the inverter failure; moreover, the disadvantage of the conventional method are its high cost and re-design problem if the inverter specification needs to be changed. Multi-level decomposition wavelet transformation is an efficient method to detect the fault location and components of the inverter. Prompt and accurate diagnostic function is possible using the normalized standard deviation of the wavelet coefficients. The proposed algorithm has simple calculation and precise diagnostic capabilities of the fault detection. A computer simulation is performed and the experimental result verifies the validity of the proposed method.

Keywords: Wavelet transform; Fault detection; Photovoltaic system; Islanding detection

1. Introduction

A typical grid-connected photovoltaic system consists of solar array, power conditioning system (PCS), local loads and a grid system with magnetic contactor and the configuration is shown in Fig. 1. The connection point between PCS and grid system is defined as Point of Common Coupling (PCC).

The major function of the PCS is to transfer solar energy (dc) into a grid system (ac) with the unity power factor using power electronics technologies. Since the dynamic and steady-state characteristics of the PV system affect their connection to the grid system, grid protection and power quality have become the major issues in the grid-connected PV system.

Islanding detection is very important issue for grid protection. It occurs when the system containing both the load and PCS remains energized by the PV system when it is isolated from the grid system, while the voltage and frequency are maintained around their nominal values. The IEEE Std. 1547-2003, specifies that the anti-islanding system must instantly disconnect the PV system within 2 s of the islanding.

In terms of the power quality issues, IEEE Std. 929-2000 specifies the recommended standards for interfacing PV systems to the grid system. The PCS output should have low current-distortion levels to ensure that no adverse effects on other equipment connected to the grid system. The PCS output at the Point of Common Coupling (PCC) should comply with Clause 10 of IEEE Std

* Tel.: +82 43 841 5142.
E-mail address: iskim@ut.ac.kr

http://dx.doi.org/10.1016/j.solener.2016.01.005
0038-092X/

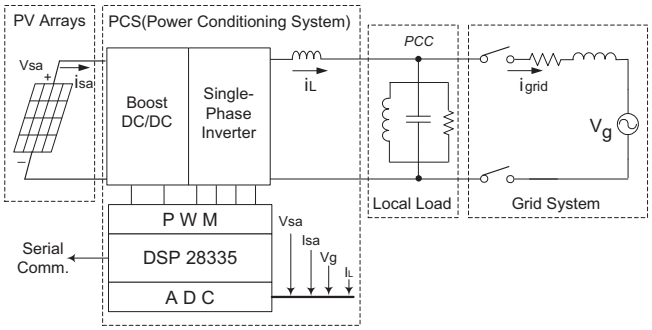

Fig. 1. Photovoltaic system configuration.

519-1992 and should be used to define the acceptable distortion levels for PV systems connected to a grid. The key requirements of this clause are summarized as follows (IEEE, 2003, 1992):

- The total harmonic current distortion shall be less than 5% of the fundamental frequency current at the rated inverter output.
- Each individual harmonic shall be limited to the percentages listed in Table 1. The limits in Table 1 are a percentage of the fundamental frequency current at full system output. Even harmonics in these ranges shall be <25% of the odd harmonic limits listed.

The PCS should be manufactured to comply with the requirements of the Std. 519-1992. If the PCS generates more harmonics than the regulation, it should be detected and the operation of the PCS should be stopped immediately to protect the grid system. Unwanted harmonics can be generated by the failures of PCS such as IGBT (Insulated Gate Bipolar Transistor) fault or a sensor or controller fault. Therefore, PCS needs to have harmonic detection capability for interfacing with the grid. Also, other kinds of faults such as islanding operation should be rapidly detected and the PCS should be disconnected from the grid network to guarantee safe operation.

Many researches have been performed on PCS fault detection. Inverter open fault detection methods have been widely researched over the past few years (Kim et al., 2009; Zidani et al., 2008; Khomfoi and Tolbert, 2007; Druant et al., 2013; Jung et al., 2013; Najafabadi et al., 2011; Akin et al., 2009; Karimi et al., 2009; Diallo et al., 2005; Silvestre et al., August 2013; Hu et al., October 2013; Peuget et al., 1998; Riberio et al., 2003; Trejo et al., 2013; Gokmen et al., 2012; Kalogirou et al., 2008). The method based on measured voltage is commonly used. However, these methods require additional voltage sensors. Kim et al. presented a method to detect open-circuit faults in a single switching device for a three-phase NPC inverter. This was achieved by measuring the pole voltage and its time period. However, this method necessitates additional circuits. Further, the location of the faulty switch could not be identified (Kim et al., 2009). Zidani et al. suggested a fuzzy-logic-based technique that detects and identifies the faulty switches in a voltage-fed PWM inverter for an induction motor drive by using Concordia current patterns. However, this method requires a relatively long diagnosis time because the dimension of the current patterns is used when the fault occurrence is determined (Zidani et al., 2008). Khomfoi and Tolbert proposed a fault diagnosis scheme to detect and identify the location of a fault in a multilevel inverter by using a neural network algorithm. However, this technique requires high computational effort (Khomfoi and Tolbert, 2007).

Table 1
Distortion limits as recommended in IEEE Std 519-1992 for six-pulse converters.

Odd harmonics	Distortion limit
3rd – 9th	<4.0%
11th – 15th	<2.0%
17th – 21st	<1.5%
23rd – 33rd	<0.6%
Above the 33rd	<0.3%

Fourier transform is the conventional method used to detect harmonics from the PCS current or voltage. It can decompose signals into frequency components with magnitude and phase. It is implemented with Discrete Fourier Transform (DFT) to convert an analog signal into digital harmonic components. The harmonic components up to the *n-th* switching frequency can be obtained. The disadvantage of the Fourier transform is that its calculation is too complex to implement into a real-time on-line application. When implemented, additional high speed signal-conditioning boards are required for the controller, which incurs a high manufacturing cost.

The wavelet transform (WT) is another way of obtaining harmonic components (Aktas and Turkmenoglu, 2010; Kim and Aggarwal, 2000; Gaouda et al., 1999; Zheng et al., 1999; Wilkinson and Cox, 1996). It employs a mother wavelet instead of orthogonal sine and cosine functions to extract frequency components. The high and low frequency components are obtained using a dyadic frequency filter. The low frequency components are decomposed into higher frequency components. It is possible to obtain signal levels at frequency bands instead of exact components. The advantage of WT is the simple calculation and it can be completed in less time than DFT.

Some applications of WT based islanding detection in grid-connected systems have been presented (Hanif et al., 2012; Pigazo et al., 2009; Wilkinson and Cox, 1996; Samui and Samantaray, Jan. 2013; Datta et al., December 2014; Perpinan and Lorenzo, 2011). The wavelet energies and their standard deviations are used to determine the islanding condition (Wilkinson and Cox, 1996).

A new fault detection algorithm of the PCS using wavelet transform is proposed in this paper. It can detect a switch open fault and any over harmonics using the Multi Level Decomposition (MLD) algorithm of the wavelet transform. The proposed algorithm can also detect an islanding condition using wavelet coefficients energies.

The advantage of the proposed algorithm is the simple calculation, which is a time correlation obtained by sequential multiplication and addition. The algorithm decomposes a measured signal at each wavelet tree level and extracts coefficients. The variations of the extracted coefficients are used to identify a fault. The simple calculation structure and fast detection time are obtained by the MLD algorithm of the wavelet transform. The brief introduction of the wavelet background is shown in the following chapter.

2. Background of wavelet transform

Since the utility system in KOREA is a 60 Hz AC power with high order harmonic components, the signal analysis is required to obtain frequency components. The Fourier analysis is the most common method that transforms time domain signals into the frequency components. It is useful for many signals, because signal frequencies have great importance to analyze the system faults. Fourier analysis is based on the orthogonal characteristics of the sine and cosine functions over a cycling period. However, the Fourier transform has a serious drawback. Time information is lost when transforming to the frequency domain. If the signal waveforms do not change significantly over time, a stationary signal is shown, and the Fourier transform is suitable. However, short time disturbances, such as drift, abrupt, swell and transient, occur in the grid system, Fourier analysis is not suited to detecting these abnormalities.

A wavelet transform is studied to correct this deficiency. A wavelet is a waveform of effectively limited duration that has an average value of zero (Hu et al., 2013).

$$W[f(a,b)] = < f, \varphi_{a,b} > = \int_{-\infty}^{\infty} f(t) \frac{1}{\sqrt{a}} \varphi^* \left(\frac{t-b}{a} \right) dt \qquad (1)$$

where a denotes scale, b denotes transition.

It is noticed that the higher scale corresponds to the most "stretched" wavelets. The more stretched the wavelet, the longer the portion to be compared, and thus the coarser the signal features being measured by the wavelet coefficients. A Transition is the movement of a window from a signal location to another point. Calculating wavelet coefficients at every scale requires lot of resources and data. If we choose scales and positions based on powers of two (called *dyadic* scale and positions), it is named as discrete wavelet transform (DWT). The terms *approximations* and *details* are widely used in DWT applications. *Approximations* are high-scale, low-frequency components and *Details* are low-scale, high-frequency components. The filtering process is expressed as follows:

$$\begin{aligned} CA_{j+1}[p] &= \sum_{n=-\infty}^{\infty} h[n-2p] CA_j[n] = CA_j * h[-2p] \\ CD_{j+1}[p] &= \sum_{n=-\infty}^{\infty} g[n-2p] CA_j[n] = CA_j * g[-2p] \end{aligned} \qquad (2)$$

where $h[.]$ is a form of low pass filter, $g[.]$ is a high pass filter and * denotes convolution. CA is approximation coefficient and CD is the detailed coefficients that result from signal convolution. The original signal, S, passes through two complementary filters (high and low pass) and decomposed into two down sampled signals, CD1 and CA1. The down sampling is necessary due to the doubled data samples. The original signal S consists of 1000 samples of data, for example, and the resulting signals CD1 and CA1 will then each have 500 samples by down sampling process. The decomposition process can be iterated, with successive approximations being decomposed in turn, so that original signal can be decomposed into many lower resolution components. This is termed a Multi-Level Decomposition (MLD) tree. Fig. 2 depicts this process.

It is very important to choose correct mother wavelet function according to the applications areas. Daubechies functions are widely used in photovoltaic applications. The DBN is the order of the Daubechies function. Fig. 3 shows the wavelet functions of the nine members of the Daubechies family. The DB2 and DB3 functions are mostly used in electrical power system analysis.

3. Fault detection algorithm

The fault detection algorithm was developed on the PCS fault cases using 3-level MLD tree. The following two cases are considered: switch open and over harmonic. The PCS transforms DC solar voltage into AC grid current using semiconductor switch such as FET (Field Effect Transistor) or IGBT. It can be considered that the switch open is caused by switching device breakdown and over harmonic is caused by a controller or sensor failure. The switch short faults cases are not considered here. When the switches are in short fault, the system is protected by the over-current limiting function or melting fuse, and PCS then stops operating. If the switches are in open fault, the PCS current has a distorted waveform and continues providing high order harmonics to the grid. The open switch fault can be classified as an UP and DOWN switch failure in the inverter bridge. The analysis result is shown in Fig. 4.

The inverter current I_{grid} waveform is shown in the first graph. The three intervals are classified as normal (I), UP switch open fault (II), and DOWN switch open fault (III). The wavelet coefficients are obtained at the starting points of the subsequent cycles. The calculated CA1, CA2, and CA3 coefficients are plotted in the second graph. It can be seen that the positive period of the coefficients is zero when the UP switch is open (II) and the negative period of the coefficients is zero when the DOWN switch is open (III). In order to clearly visualize the wavelet

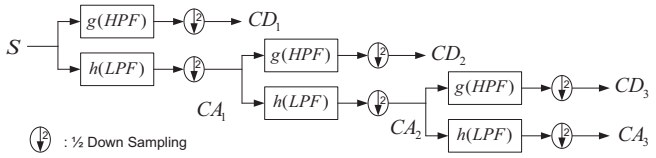

Fig. 2. Multi-level Decomposition tree.

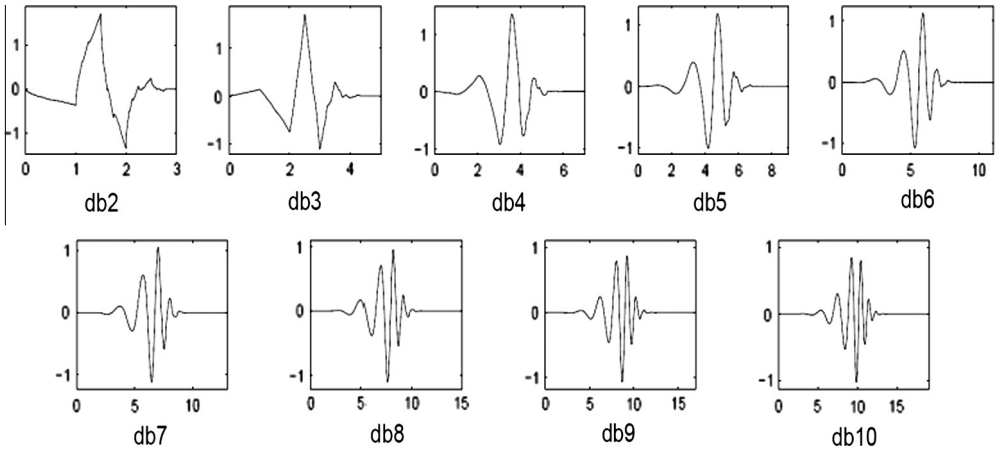

Fig. 3. Wavelet functions of Daubechies.

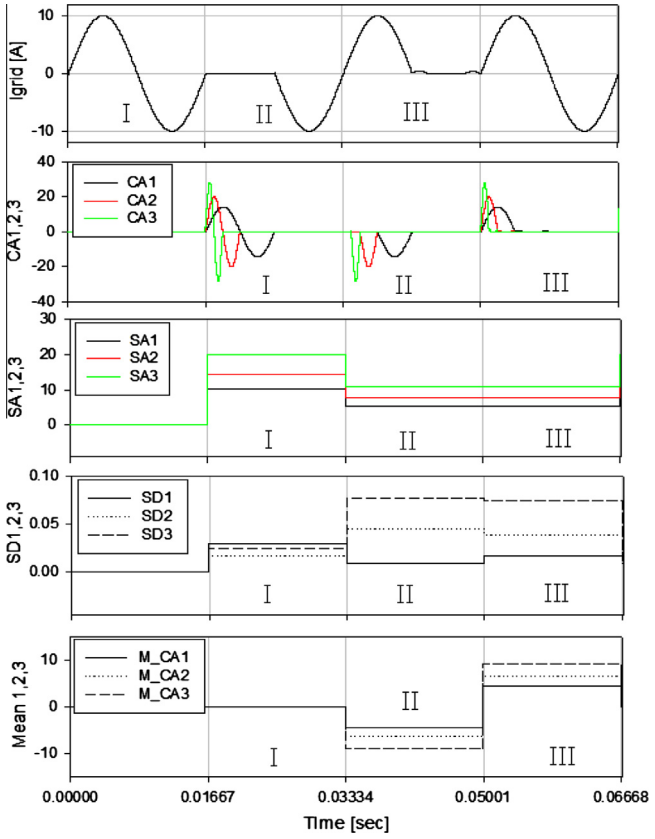

Fig. 4. Switch open fault analysis.

coefficient changes over the fault conditions, the concept of standard deviation was introduced in this paper. Distortions occurring in the wavelet coefficients can result an increase or decrease of standard deviations.

The standard deviation of coefficients of X ($X = A$ or D) is defined SX_i. The SA_i is defined as the normalized standard deviation of the coefficients of the *Approximation* CA_i and SD_i is defined as the normalized standard deviation of the coefficients of the *Detail* CD_i. And its expression is shown as follows:

$$SX_i = \sqrt{\frac{\sum_{k=1}^{n}(CX_i(k) - CX_i(mean))^2}{n}} \tag{3}$$

where $CX_i(mean) = \frac{CX_i(1)+CX_i(2)+\cdots CX_i(n)}{n}$, n is a sample number where CX_1 is 128, CX_2 is 64 and CX_3 is 32. The normalized standard deviation of the SX_i is defined as follows:

$$\eta(SX_i) = \frac{SX_i - SX_{i,normal}}{SX_{i,normal}}, \quad SX_i = SA_1, SA_2, SA_3, SD_1, SD_2, SD_3 \tag{4}$$

where $SX_{i,\ normal}$ is defined as the standard deviation at normal operation period (I).

The figure of standard deviation (SA1, SA2, SA3 and SD1, SD2, SD3) are shown in the third and fourth graph. The step jump can be seen during the fault conditions. The SA1, SA2, and SA3 do not change during the (II) and (III) periods. Also SD1, SD2, and SD3 have few changes in both periods. The normalized SA and SD are summarized in Table 2. Since η(SA3) and η(SD3) have more distinct changes than η(SA1, SA2) and η(SD1, SD2), it is much easier to distinguish their fault conditions from a normal operation.

While η(SA3) and η(SD3) can identify a switch open fault, it is not suitable for the SA3 and SD3 values to distinguish the location of a switch fault. The fault location can be found by observing the means of the wavelet coefficients. The means of the CA1, CA2, and CA3 coefficients are shown in the fifth graph. It can be seen that it has a negative mean during period (II) and a positive mean during

Table 2
Normalized standard deviation for open fault conditions.

Normalized SD	II (UP)	III (DOWN)
$\eta(SA_1)$	−0.454	−0.458
$\eta(SA_2)$	−0.455	−0.460
$\eta(SA_3)$	−0.455	−0.460
$\eta(SD_1)$	−0.693	−0.433
$\eta(SD_2)$	1.611	1.273
$\eta(SD_3)$	2.151	2.043

period (III). Therefore, the switch fault condition can be easily detected by observing the standard variation and mean of the CA and CD coefficients.

The over harmonic faults cases are analyzed in Fig. 5. Period A is defined as a normal operation, period B is defined as a spike-up, period C is defined as a spike-down and period D is defined as a high harmonic, as shown in the first figure. The spike-up and down operation can be caused by the intermittent short in the inverter bridge, and high harmonic can be caused by controller or sensor fault.

The waveforms of CA1, CA2, and CA3 are shown in the subsequent graphs of Fig. 5. The standard deviation for the SA1, SA2, SA3 and SD1, SD2, SD3 waveforms are shown in the fifth and sixth graph, respectively. The SA1, SA2, and SA3 do not show significant changes during the B, C, and D periods. The SD1, SD2, and SD3 show large changes. The SD3 has larger changes than SD1 and SD2 for all periods. The plot for normalized standard deviation is shown in Fig. 6. The η(SD3) has a relatively high value compared with other coefficients, and thus it can be an over harmonic index. It can be inferred from the fact that the high frequency components of the over harmonic waveforms have higher detail number than approximation due to their residing frequency bands. Higher detail number has high standard deviations than approximation. It's the reason over harmonic waveforms shows higher standard deviations in the detail rather than approximation.

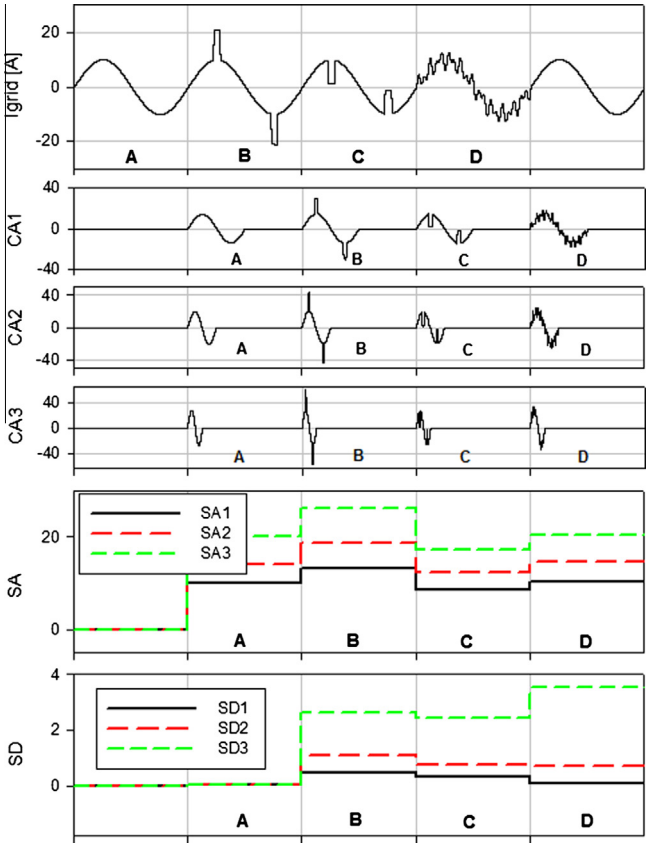

Fig. 5. Analysis for over harmonic faults.

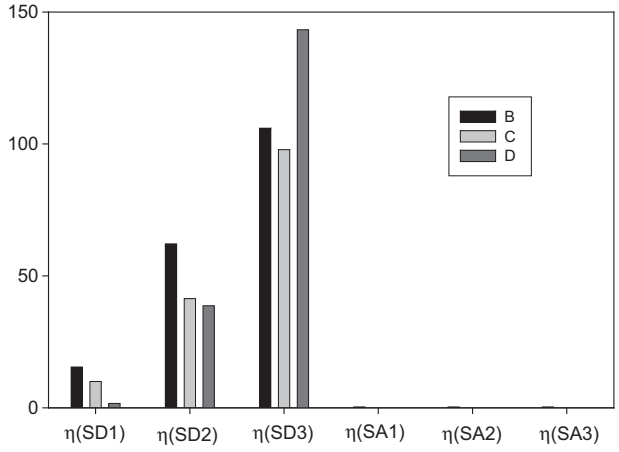

Fig. 6. Normalized standard deviation of over harmonic generation.

An islanding detection algorithm is developed. It is based on the fact that when the grid fails, large impedance changes occur in the grid voltage, positioning the harmonic components outside of the threshold range for detection. Therefore, the islanding condition can be identified by observing the CD coefficients.

The spectral energy of the wavelet coefficients for a given window of length L is defined as

$$E_n = \frac{\sum_{k=1}^{L} C_n^2}{L} \tag{5}$$

where L is the number of samples for a one cycling period of the PCC voltage.

The islanding condition can be detected by comparing subsequent corresponding energy levels for one cycle of grid voltage.

4. Experimental result

PCS has a cascade configuration with a boost converter and grid-connected inverter. The boost converter is used to step-up the solar array voltage to the desired DC link voltage so that it is sufficiently high to transfer solar energy into the grid. The solar array information, such as the voltage and current, are sensed to control maximum power tracking. The grid voltage is sensed through PCC to be synchronized with the Phase Locked Loop (PLL) control. The inductor current is also sensed to achieve a unity power factor with the grid voltage. The block diagram of the controller is shown in Fig. 7. The PCS controller is built using a 32-bit floating point DSP based microcontroller TMS320F28335. High accuracy bipolar input (±10 V) simultaneous 6-channel external ADC boards are manufactured to obtain precise signal conversion. The controller can transmit internal data, such as wavelet coefficients or energy, into the PC via high speed serial communication.

The sampling frequency is set to 15,360 Hz for a 60 Hz grid signal to obtain the 2s power of the sample number of the 256 samples. The number of samples is 256 for the first level, 128 for the second level, and 64 for the third level, by

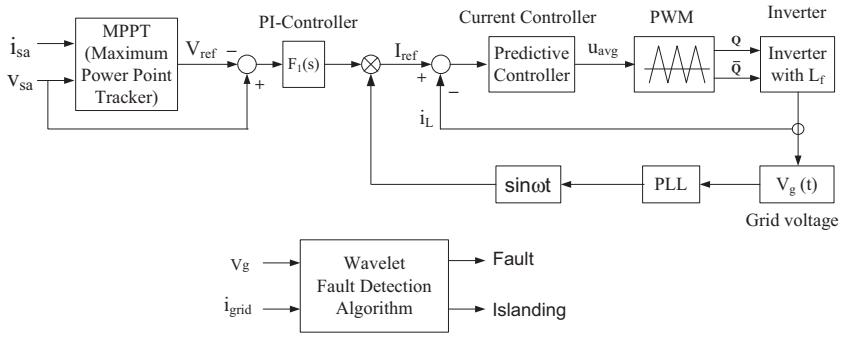

Fig. 7. The block diagram of the controller.

down sampling. When the grid voltage crosses the zero point, the sampling index is reset to zero and new sampling is starting. The stored 256 point samples for the last cycle were converted into wavelet coefficients by multi-level decomposition. The algorithm for fault detection and islanding detection is also executed at this stage. The flowchart for the algorithm is shown in Fig. 8. The waveform of MLD for the grid voltage is shown in Fig. 9. The upper waveform is the grid voltage and the subsequent figures show CA1, CA2 and CA3. It can be seen that the waveforms are stretched down to half due to the down sampling at each decomposition level. The magnitudes of high frequency components, such as CD1, CD2 and CD3, are so small that it is hard to find their differences in the oscilloscope.

The experimental result for UP switch open fault condition is shown in Fig. 10. The first figure shows output current, second figure is CD1, third figure is CD2 and the last figure is CA3. When open fail happens, the positive part of the grid current is goes to zero. The coefficients of the detail changed a little, however the coefficients of the approximation shows a large changes in the waveforms.

In order to find the switch open fault condition, the graph for S(CA3), S(CA1) and S(CD1) are shown in Fig. 11. It can be seen that the experimental result shows the same results as in the simulation.

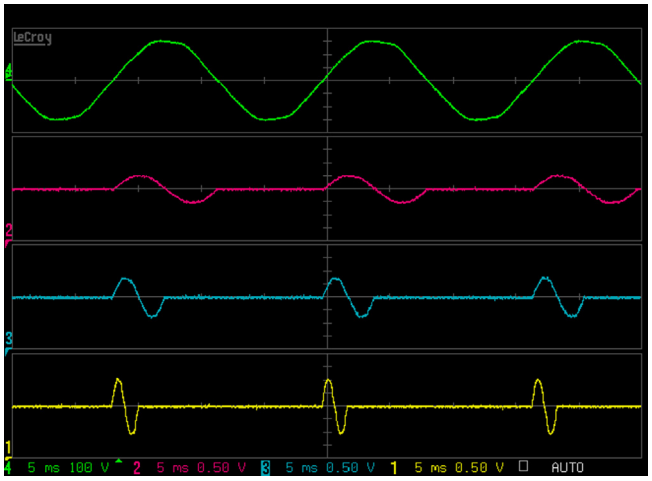

Fig. 9. DWT waveform. (Upper: Vgrid, Middle: CA1, CA2, Bottom: CA3).

The harmonic distortion condition is shown in Fig. 12. The 11th, 13th, and 19th harmonics are included in the

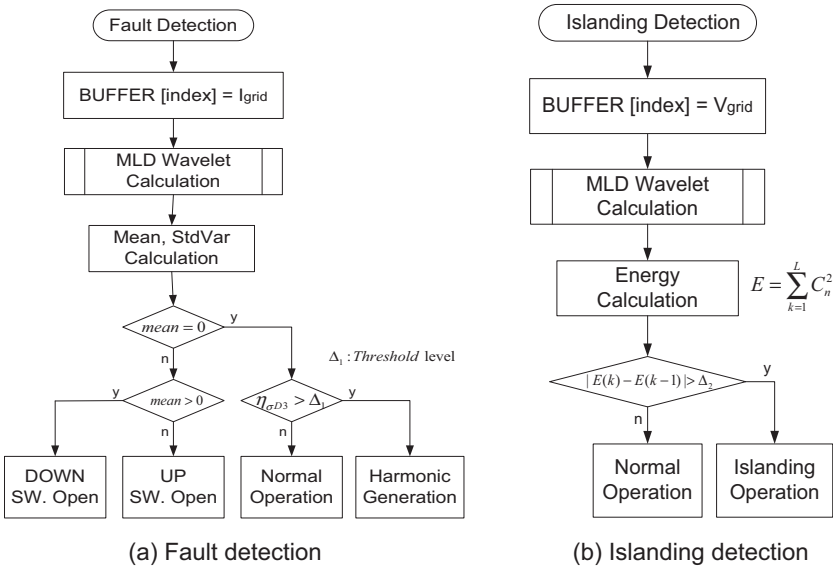

(a) Fault detection (b) Islanding detection

Fig. 8. Algorithm for fault detection and islanding detection.

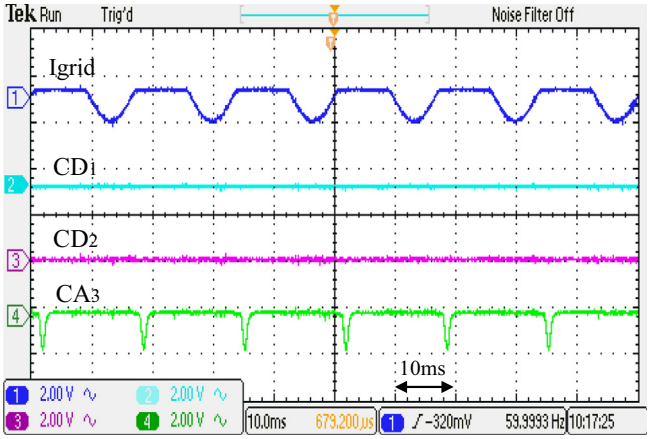

Fig. 10. Wavelet waveform during open fail case.

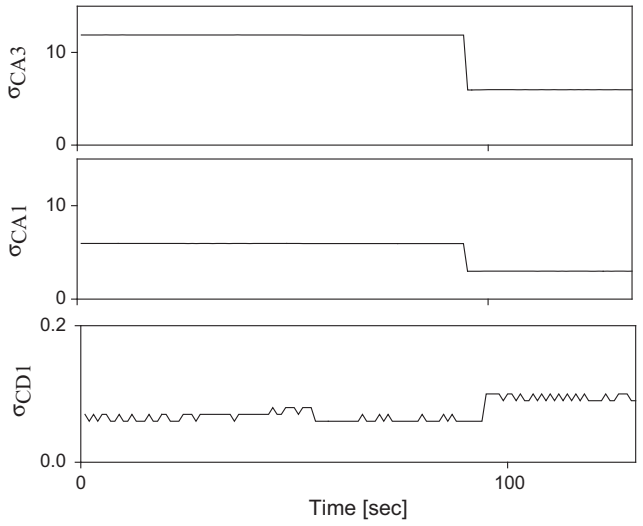

Fig. 11. Std. deviation waveform for open fault.

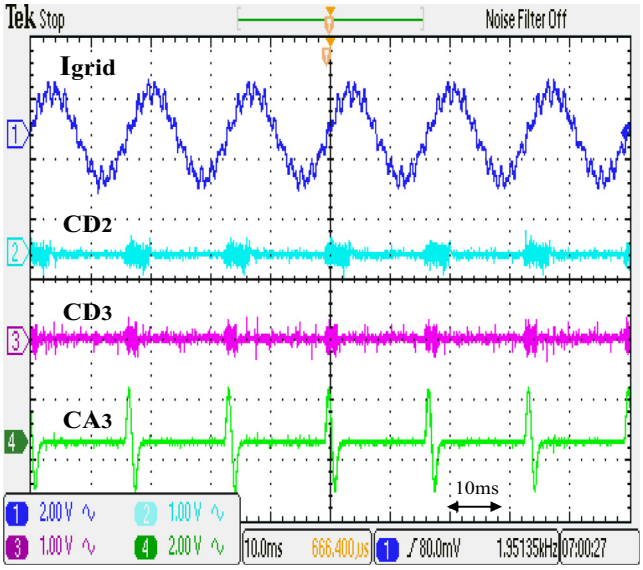

Fig. 12. Wavelet waveform during harmonic generation.

PCS current to demonstrate the over harmonic condition. The first figure shows grid current, second figure is CD2, third figure is CD3 and the last figure is CA3. In order to find the over harmonic condition, the graph for S(CA3), S(CD2) and S(CD3) are shown in Fig. 13 using PC transmitted data obtained from experimental result. The variations of the standard deviation show same trends as those of the simulation. The PC stored coefficients plots are shown in Fig. 13. The harmonic condition can be detected from the CD3 changes.

It can be seen that the Fig. 13 shows the same results of the simulation Fig. 5 (period C). Since high detail coefficients have high standard deviations than approximation, it's the reason why over harmonic waveforms shows higher standard deviations in the detail rather than approximation.

The wavelet energy during islanding is shown in Fig. 14. The grid voltage is placed under a normal operation condition, ranging from 215 to 218 Vac. The conventional methods have failed to detect islanding conditions because the grid voltage lies in the normal operating ranges. The proposed wavelet energy methods can show superior performance in this operating condition. The grid voltage is measured at 65 [μs] intervals and calculate wavelet coefficients at the zero crossing point of the voltage. The coefficients were converted into energies using the proposed equations. The wavelet energies for the three-level decomposition (CA1, 2, 3 and CD1, 2, 3) are shown in the figure. It can be seen that the energy levels are step changed when islanding occurs. The amount of energy change depends on the grid and local load conditions. Considering the operating conditions of the utility system, the rate of change of grid and local load conditions is limited to 10–20%. Therefore, it is reasonable to select 50% of the boundary condition for the energy level changes during the islanding operations.

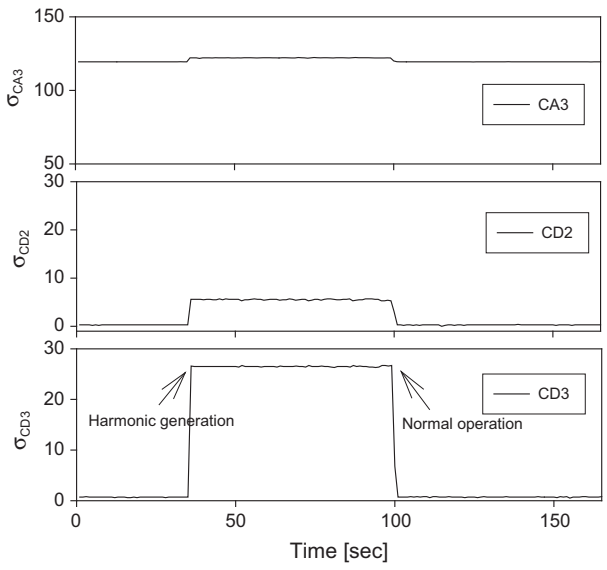

Fig. 13. Wavelet std. change when the harmonic has occurred.

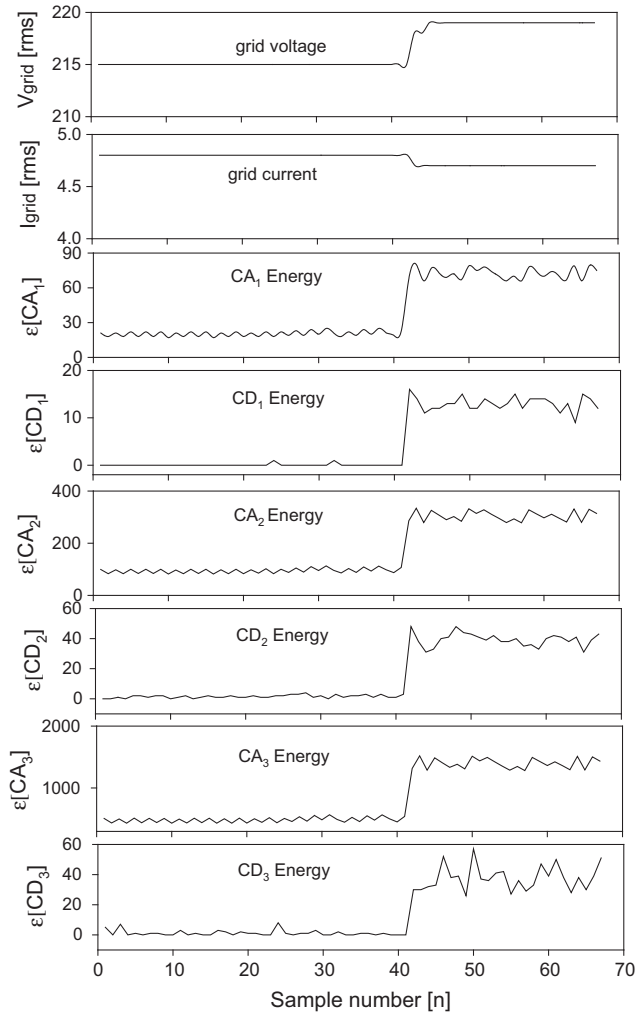

Fig. 14. Wavelet Energy changes during islanding condition.

5. Conclusion

In this paper, the fault detection algorithm for PCS in real time is studied. The fault identification was performed using the multi level decomposition method. The wavelet coefficients changes are used as a fault classifying method. The advantage of the proposed methods is the simple structure without any hardware changes. It can be implemented by adding software codes. The simulation and experimental result show the excellent performance of the proposed system. The field tests will be performed to verify the suggested algorithm for further works.

Acknowledgement

This research was supported by Basic Science Research Program through the National Research Foundation of Korea (NRF) funded by the Ministry of Education [2014R1A1A2056443].

References

Akin, B., Ozturk, S.B., Toliyat, H.A., Rayner, M., 2009. DSP-based sensorless electric motor fault-diagnosis tools for electric and hybrid electric vehicle power train applications. Vehicular Technol., IEEE Trans. 58 (6), 2679–2688.

Aktas, M., Turkmenoglu, V., 2010. Wavelet-based switching faults detection in direct torque control induction motor drives. IET Sci. Meas. Technol. 4 (6), 303–310.

Datta, A., Saha, D., Ray, A., Das, P., 2014. Anti-islanding selection for grid-connected solar photovoltaic system applications: A MCDM based distance approach. Sol. Energy 110, 519–532. http://dx.doi.org/10.1016/j.solener.2014.12.08.

Diallo, D., Benbouzid, M.H., Hamad, D., Pierre, X., 2005. Fault detection and diagnosis in an induction machine drive: a pattern recognition approach based on Concordia stator mean current vector. Energy Conversion, IEEE Trans. 20 (3), 512–519.

Druant, J., Vyncke, T.K., Melkbeek, J.A., 2013. Adding inverter fault detection to model-based predictive control for flying-capacitor inverters. In: Sensorless Control for Electrical Drives and Predictive Control of Electrical Drives and Power Electronics (SLED/PRECEDE), 2013 IEEE International Symposium.

Gaouda, A.M., Safama, M.M.A., et al., 1999. Power quality detection and classification using wavelet-multi resolution signal decomposition. IEEE Trans. Power Deliv. 14 (4), 1469–1476.

Gokmen, N., Karatepe, E., Celik, B., Silvestre, S., 2012. Simple diagnostic approach for determining of faulted PV modules in string based PV arrays. Sol. Energy 86 (11), 3364–3377. http://dx.doi.org/10.1016/j.solener.2012.09.007.

Hanif, M., Basu, M., Gaughan, K., 2012. Development of EN50438 compliant wavelet-based islanding detection technique for three-phase static distributed generation systems. IET Renew. Power Gener. 6 (4), 289–301.

Hu, Y., Song, X., Tian, G., He, Z., 2013. Photovoltaic fault detection using a parameter based model. Sol. Energy 96, 96–102. http://dx.doi.org/10.1016/j.solener.2013.07.004.

IEEE Recommended Practices and Requirements for Harmonic Control in Electrical Power Systems, IEEE Std. 519-1992, 1992.

IEEE Standard for Interconnecting Distributed Resources with Electric Power Systems, IEEE 1547, Jul. 28, 2003.

Jung, S.M., Park, J.S., Kim, H.W., et al., 2013. An MRAS-based diagnosis of open-circuit fault in PWM voltage-source inverters for PM synchronous motor drive systems. Power Electron., IEEE Trans. 28 (5), 2514–2526.

Kalogirou, S., Lalot, S., Florides, G., Desmet, B., 2008. Development of a neural network-based fault diagnostic system for solar thermal applications. Sol. Energy 82 (2), 164–172. http://dx.doi.org/10.1016/j.solener.2007.06.010.

Karimi, S., Poure, P., Saadate, S., 2009. Fast power switch failure detection for fault tolerant voltage source inverters using FPGA. IET Power Electron. 2 (4), 346–354.

Khomfoi, S., Tolbert, L.M., 2007. Fault diagnostic system for a multilevel inverter using a neural network. Power Electron., IEEE Trans. 22 (3), 1062–1069.

Kim, Chul Hwan, Aggarwal, Raj, 2000. Wavelet transform in power systems. Power Eng. J., 81–87

Kim, T.J., Lee, W.C., Hyun, D.S., 2009. Detection method for open-circuit fault in neutral-point-clamped inverter systems. Ind. Electronics, IEEE Trans. 56 (7), 2754–2763.

Najafabadi, T.A., Salmasi, F.R., Maralani, P.J., 2011. Detection and isolation of speed-, DC-link voltage and current-sensor faults based on an adaptive observer in induction-motor drives. Ind. Electron., IEEE Trans. 58 (5), 1662–1672.

Perpinan, O., Lorenzo, E., 2011. Analysis and synthesis of the variability of irradiance and PV power time series with the wavelet transform. Sol. Energy 85 (1), 188–197. http://dx.doi.org/10.1016/j.solener.2010.08.013.

Peuget, R., Courtine, S., Rognon, K.P., 1998. Fault detection and isolation on a PWM inverter by knowledge-based model. Ind. Appl., IEEE Trans. 34 (6), 1318–1326.

Pigazo, A., Liserre, M., Mastromauro, R.A., et al., 2009. Wavelet-based islanding detection in grid-connected PV system. IEEE Trans. Ind. Electron. 56 (11), 4445–4455.

Riberio, R.L., Jacobina, C.B., Silva, E.R., Lima, A.M., 2003. Fault detection of open-switch damage in voltage-fed PWM motor drive systems. Power Electron., IEEE Trans. 18 (2), 587–593.

Samui, A., Samantaray, S.R., 2013. Wavelet singular entropy-based islanding detection in distributed generation. IEEE Trans. Power Deliv. 28 (1), 411–418.

Silvestre, S., Chouder, A., Karatepe, E., 2013. Automatic fault detection in grid connected PV systems. Sol. Energy 94, 119–127. http://dx.doi.org/10.1016/j.solener.2013.05.001.

Trejo, D.R., Delgado, D.U., Bossio, G., et al., 2013. Fault diagnosis scheme for open-circuit faults in field-oriented control induction motor drives. IET Power Electron. 6 (5), 869–877.

Wilkinson, W.A., Cox, M.D., 1996. Discrete wavelet analysis of power system transients. IEEE Trans. Power Deliv. 11 (4), 2038–2044.

Wilkinson, W.A., Cox, M.D., 1996. Discrete wavelet analysis of power system transients. IEEE Trans. Power Deliv. 11 (4), 2038–2044.

Zheng, Tongxin, Makram, Elham B., Girgis, A.G., 1999. Power system transient and harmonic studies using wavelet transform. IEEE Trans. Power Deliv. 14 (4), 1461–1468.

Zidani, F., Diallo, D., Benbouzid, M.H., 2008. A fuzzy-based approach for the diagnosis of fault modes in a voltage-fed PWM inverter induction motor drive. Ind. Electronics, IEEE Trans. 55 (2), 586–593.